Signatures of Exciton Orbits in Quantum Mechanical Recurrence Spectra of Cu₂O

Jan Ertl [1,2] Michael Marquardt,[1] Moritz Schumacher,[1] Patric Rommel,[1] Jörg Main,[1,*] and Manfred Bayer[2]

[1]*Institut für Theoretische Physik I, Universität Stuttgart, 70550 Stuttgart, Germany*
[2]*Experimentelle Physik 2, Technische Universität Dortmund, 44221 Dortmund, Germany*

The seminal work by Kazimierczuk *et al.* [Nature **514**, 343 (2014)] has shown the existence of highly excited exciton states in a regime, where the correspondence principle is applicable and quantum mechanics turns into classical mechanics; however, any interpretation of exciton spectra based on a classical approach to excitons is still missing. Here, we close this gap by computing and comparing quantum mechanical and semiclassical recurrence spectra of cuprous oxide. We show that the quantum mechanical recurrence spectra exhibit peaks, which, by application of semiclassical theories and a scaling transformation, can be directly related to classical periodic exciton orbits. The application of semiclassical theories to exciton physics requires the detailed analysis of the classical exciton dynamics, including *three-dimensional* orbits, which strongly deviate from hydrogenlike Keplerian orbits. Our findings illuminate important aspects of excitons in semiconductors by directly relating the quantum mechanical band structure splittings of excitons to the corresponding classical exciton dynamics.

Excitons are atomlike states in semiconductors formed by an electron and a positively charged hole. They are created by exciting an electron from the valence band into the conduction band, where the electron forms a bound hydrogenlike state with the hole remaining in the valence band [1,2]. Since the experimental observation of giant Rydberg excitons with principal quantum numbers up to $n = 25$ in Cu₂O by Kazimierczuk *et al.* [3] the exciton physics of cuprous oxide has attracted a strongly increasing interest, both experimentally [3–6] and theoretically [4–8]. In particular, the impact of the valence band structure causes significant deviations of the exciton spectra from a simple hydrogenlike model, which have now been investigated in great detail [4–7].

For the hydrogen atom the connection of Rydberg spectra to classical Keplerian orbits is well established by the Bohr-Sommerfeld model. Semiclassical trace formulas [9,10] provide the link between quantum spectra and classical dynamics of both regular and chaotic systems, and are the foundation for the understanding of level-spacing dynamics [11]. For example, the diamagnetic Kepler problem has served as a prototype system for the study of *quantum chaos*, i.e., the effects of a classical chaotic dynamics on quantum spectra [12,13]. Because of the additional spin degrees of freedom in the semiconductor and the strong, non-negligible spin-orbit interaction the existence of an exciton dynamics for quasiparticles similar to that for electrons in hydrogen atoms is not obvious. A first step on a semiclassical description of Rydberg excitons in Cu₂O has been made in Ref. [14] by proposing a classical model using an adiabatic approach that separates the fast spin dynamics and the slow electron-hole dynamics. By constructing action variables for the exciton dynamics in certain symmetry planes of the crystal allowed energy regions for the existence of exciton states could be obtained. This gives a first hint for the validity of a semiclassical approach; however, a direct verification of a classical exciton dynamics is still missing. By computing the quantum mechanical recurrence spectra and comparing them with the classical and semiclassical results, we reveal the existence and meaningfulness of a classical exciton dynamics. Direct signatures of exciton orbits obtained in quantum mechanical exciton recurrence spectra provide an intuitive picture for the understanding of excitons in Cu₂O.

The investigation of the phase space topology with similar methods, as introduced by Gekle *et al.* [15,16] for the hydrogen atom in crossed electric and magnetic fields, reveals a mostly regular or near-integrable exciton dynamics with periodic orbits on one- to three-dimensional tori. Here, we establish the connection between the fine-structure splitting of excitons in quantum spectra of the yellow series of Cu₂O and the corresponding classical exciton dynamics. According to semiclassical theories [9,10], the frequencies of the oscillations are determined by the action of the periodic orbits, and the amplitudes are related to stability properties of the orbits at a given energy. Performing a Fourier transform of the density of states from energy to time domain results in a recurrence spectrum which exhibits peaks at periods that can be assigned to classical orbits, as shown in Sec. I of the Supplemental Material [17]. For systems exhibiting an appropriate scaling property the peaks in the recurrence spectrum become sharp δ peaks [26]. To this aim we apply a scaling technique and calculate the classical dynamics of the

system. The obtained periodic exciton orbits perfectly explain the observed structures in the quantum mechanical recurrence spectra, and thus provide a deeper physical understanding of excitons in semiconductors.

A full description of excitons in cuprous oxide needs to consider the cubic O_h symmetry of the system. Introducing relative and center-of-mass coordinates for the electron and hole and neglecting the center-of-mass momentum, the Hamiltonian for excitons in cuprous oxide is given by [7,27,28]

$$H = E_g + H_{\mathrm{kin}}(\boldsymbol{p}, \hat{\boldsymbol{I}}, \hat{\boldsymbol{S}}_h) - \frac{e^2}{4\pi\varepsilon_0\varepsilon|\boldsymbol{r}|} + H_{\mathrm{SO}}, \quad (1)$$

with the relative coordinates $\boldsymbol{r}$ and momenta $\boldsymbol{p}$ and the vector operators $\hat{\boldsymbol{I}}$, $\hat{\boldsymbol{S}}_h$ for angular momenta $I = 1$ and $S_h = 1/2$. Here, the first term $E_g = 2.17208$ eV is the gap energy between the uppermost valence band and the lowest conduction band [3]. The second term

$$H_{\mathrm{kin}}(\boldsymbol{p}, \hat{\boldsymbol{I}}, \hat{\boldsymbol{S}}_h) = \frac{\gamma_1'}{2m_0}\boldsymbol{p}^2 + \frac{1}{2\hbar^2 m_0}[4\gamma_2\hbar^2\boldsymbol{p}^2 - 6\gamma_2(p_1^2\hat{I}_1^2 + \mathrm{c.p.}) - 12\gamma_3(\{p_1, p_2\}\{\hat{I}_1, \hat{I}_2\} + \mathrm{c.p.})$$
$$- 12\eta_2(p_1^2\hat{I}_1\hat{S}_{h1} + \mathrm{c.p.}) + 2(\eta_1 + 2\eta_2)\boldsymbol{p}^2(\hat{\boldsymbol{I}} \cdot \hat{\boldsymbol{S}}_h) - 12\eta_3(\{p_1, p_2\}(\hat{I}_1\hat{S}_{h2} + \hat{I}_2\hat{S}_{h1}) + \mathrm{c.p.})], \quad (2)$$

accounts for the kinetic energy of the electron and hole. It includes the cubic band structure, described by the quasispin $\hat{\boldsymbol{I}}$ and the hole spin $\hat{\boldsymbol{S}}_h$ with their components $\hat{I}_i$, $\hat{S}_{hi}$ as well as the components of the momentum p_i. Furthermore, m_0 is the free-electron mass, $\{a, b\} = \frac{1}{2}(ab + ba)$ denotes the symmetrized product, c.p. stands for cyclic permutation, γ_i and η_i are the Luttinger parameters [5], and $\gamma_1' = \gamma_1 + m_0/m_e = 2.77$. The third term in Eq. (1) is the screened Coulomb potential with the dielectric constant $\varepsilon = 7.5$. The fourth term in Eq. (1) is the spin-orbit term

$$H_{\mathrm{SO}} = \frac{2}{3}\Delta\left(1 + \frac{1}{\hbar^2}\hat{\boldsymbol{I}} \cdot \hat{\boldsymbol{S}}_h\right), \quad (3)$$

where $\Delta = 0.131$ eV is the spin-orbit coupling [5]. In our computations we use the same material parameters as given in Ref. [29], but neglect central-cell corrections [8,30,31], which can be justified for high principal quantum numbers in the semiclassical limit, as shown in Sec. II of the Supplemental Material [17]. For a given energy the classical dynamics of the yellow exciton series can be calculated by using the adiabatic approach introduced in Refs. [14,17].

Without the spin-orbit term [Eq. (3)] the Hamiltonian [Eq. (1)] does not depend on the energy when multiplied by n_{eff}^2 and performing a scaling transformation $\boldsymbol{r} = n_{\mathrm{eff}}^2\tilde{\boldsymbol{r}}$, $\boldsymbol{p} = n_{\mathrm{eff}}^{-1}\tilde{\boldsymbol{p}}$, with the effective quantum number n_{eff} given by $n_{\mathrm{eff}}^2 \equiv E_{\mathrm{Ryd}}/(E_g - E)$ with $E_{\mathrm{Ryd}} = 13.6$ eV$/(\gamma_1'\varepsilon^2) \approx 87$ meV the Rydberg energy of cuprous oxide, which means that the classical dynamics is the same for all values of n_{eff}. The nonscaled action S is connected to the scaled value $\tilde{S}$ by a simple linear scaling $S(n_{\mathrm{eff}}) = \tilde{S}n_{\mathrm{eff}}$. In semiclassical theories the density of states for systems with such a scaling property can be expressed as a Fourier series in the scaled action $\tilde{S}_{\mathrm{PO}}$ [17,26],

$$\varrho(n_{\mathrm{eff}}) = \varrho_0(n_{\mathrm{eff}}) + \Re\sum_{\mathrm{PO}}\mathcal{A}_{\mathrm{PO}}\exp(i\tilde{S}_{\mathrm{PO}}n_{\mathrm{eff}}/\hbar), \quad (4)$$

with $\varrho_0(n_{\mathrm{eff}})$ the average density of states. The sinusoidal fluctuations of the density are related to the periodic orbits (PO) of the classical system with $\mathcal{A}_{\mathrm{PO}}$ and $\tilde{S}_{\mathrm{PO}}$ the amplitude (including the Maslov index) and the scaled action of the orbits, respectively.

To recover the scaling property for the Hamiltonian we introduce an energy-dependent coupling parameter $\tilde{\Delta}$, i.e.,

$$\Delta \to \tilde{\Delta} = \frac{n_0^2}{n_{\mathrm{eff}}^2}\Delta, \quad (5)$$

with a fixed parameter n_0. Note that the replacement [Eq. (5)] is not possible in an experiment; however, a tunable spin-orbit coupling Δ has already been used for the theoretical investigation of the exchange interaction in the yellow exciton series [31]. The classical dynamics is then that of $n_{\mathrm{eff}} = n_0$. Using the adiabatic approach [14,17] and choosing the lowest-lying energy surface in momentum space corresponding to the yellow exciton series classical exciton orbits can be obtained by numerical integration of Hamilton's equations of motion for the relative coordinates and momenta. In most parts of the phase space we observe a regular dynamics of the excitons on one- to three-dimensional tori. Periodic orbits on these tori can be described by one to three integer winding numbers M_i. The number of winding numbers for the three-dimensional orbits can be reduced to an effective two-dimensional description by two winding numbers M_1 and M_2 (Sec. II, Supplemental Material [17]). The corresponding action variables are J_1 and J_2. At given energy E they are related by the function $g_E(J_1) = J_2$, which can be used to compute the semiclassical amplitudes of periodic orbits on resonant tori [9,32]. In addition the stability eigenvalues λ_{PO}, which describe the linearized response of a periodic

orbit to a small perturbation are required for the calculation of the semiclassical amplitudes in Eq. (4). Since only one pair of stability eigenvalues shows deviations from the integrable behavior for the majority of orbits we use a mixed approach combining the amplitudes of the Berry-Tabor formula for a two-dimensional system [9,32] with the contribution of the stability eigenvalues λ_{PO} and $1/\lambda_{PO}$ for the unstable direction from Gutzwiller's trace formula [10], resulting in the equation

$$|\mathcal{A}_{PO}| = \frac{1}{\pi\hbar} \frac{1}{\sqrt{|\lambda_{PO} + 1/\lambda_{PO} - 2|}} \frac{\tilde{S}_{PO}}{\sqrt{\hbar M_2^3 |g_E''|}} \quad (6)$$

for the periodic-orbit amplitudes (Sec. II, Supplemental Material [17]). For the computation of the amplitudes of the isolated nearly circular orbits we resort directly to Gutzwiller's trace formula.

In the quantum mechanical case the operators for position and momentum read as $\hat{\tilde{r}} = \tilde{r}$, $\hat{\tilde{p}} = -i\hbar_{eff}\nabla_{\tilde{r}}$, with $\hbar_{eff} = \hbar/n_{eff}$ an effective Planck constant, as shown in Sec. III of the Supplemental Material [17]. The Schrödinger equation for cuprous oxide is now transformed to the generalized eigenvalue problem

$$\left[\frac{e^2}{4\pi\varepsilon_0\varepsilon|\tilde{r}|} - n_0^2 H_{SO} - E_{Ryd}\right]|\Psi\rangle = \hbar_{eff}^2 H_{kin}|\Psi\rangle \quad (7)$$

for the squared effective Planck constant, i.e., $\lambda = \hbar_{eff}^2$, and thus for the effective quantum number n_{eff}. Equation (7) is solved numerically by using a complete set of basis states $|NLJFM_F\rangle$ with Coulomb-Sturmian radial functions $U_{NL}(r)$ (Sec. III, Supplemental Material [17]).

The decisive point of the scaling is that the eigenvalues in Eq. (7) correspond to the effective Planck constant $\hbar_{eff} = \hbar/n_{eff}$, i.e., the eigenstates approach the semiclassical limit with increasing eigenvalues n_{eff}, but the classical exciton dynamics corresponding to the spectrum does not depend on this effective Planck constant, and thus stays the same for all states of the scaled spectrum. The classical exciton dynamics is that of the nonscaled Hamiltonian (1) [$n_{eff} = n_0$ in Eq. (5)] at energy $E = E_g - E_{Ryd}/n_0^2$, and is thus controlled via the parameter n_0 in Eqs. (5) and (7). The fluctuations of the scaled quantum spectra obtained from Eq. (7) can be analyzed by Fourier transform in the variable n_{eff} and, via the semiclassical result [Eq. (4)], should provide δ peaks at frequencies given by the scaled actions $\tilde{S}_{PO}$ of the periodic orbits of the corresponding classical exciton dynamics.

In the following all parameters are given in exciton-Hartree units which are obtained by setting $\hbar = e = m_0/\gamma_1' = 1/(4\pi\varepsilon_0\varepsilon) = 1$. For the presentation of the results we focus on $n_0 = 5$, i.e., a principal quantum number, which is high enough that the adiabatic approach is valid, but low enough that the secular motion of the classical exciton orbits, which decreases with increasing n_0, is
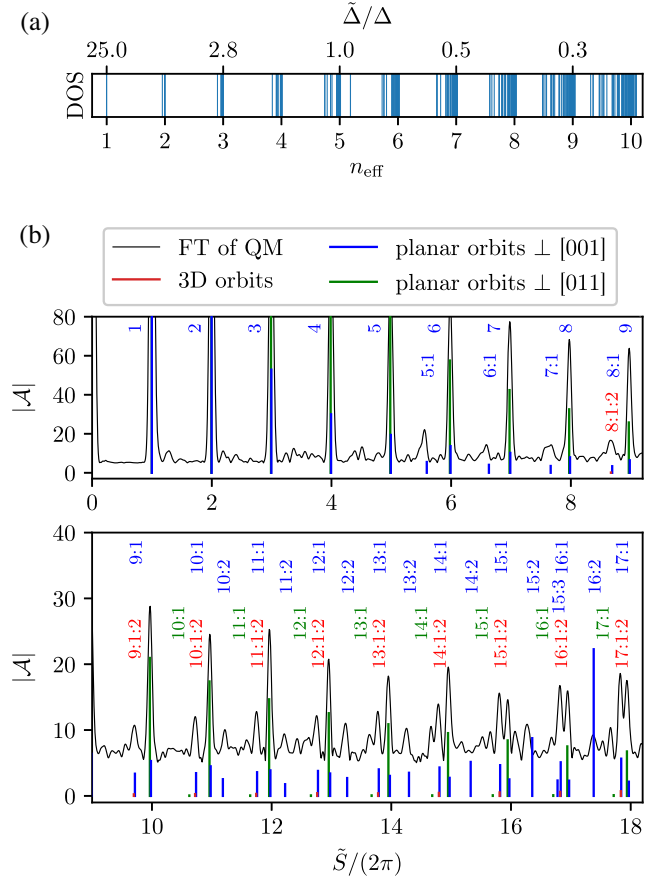
FIG. 1. (a) Part of the scaled quantum mechanical density of states (QM) for $n_0 = 5$. (b) Quantum mechanical exciton recurrence spectrum (black solid line, with zero line shifted for better visibility) obtained by FT of the QM density of states shown in (a) and the semiclassical recurrence spectrum (colored bars). The peaks corresponding to one or multiple repetitions of nearly circular orbits are labeled with a single winding number M_1. Two winding numbers $M_1:M_2$ indicate planar orbits in one of the two different symmetry planes of the crystal, and fully three-dimensional orbits are marked by three winding numbers $M_1:M_2:M_3$. The observed structures agree very well with the semiclassical results.

sufficiently fast (Sec. II, Supplemental Material [17]). Numerical diagonalization of the generalized eigenvalue problem [Eq. (7)] provides the scaled quantum mechanical spectrum for n_{eff} displayed in Fig. 1(a) showing nicely the fine structure splittings. Due to the scaling property introduced in Eq. (5) the spectrum differs from the physical (nonscaled) spectrum. The ratio of the scaled spin-orbit splitting $\tilde{\Delta}$ to the physical value Δ is shown in the upper axis of Fig. 1(a). In the vicinity of $n_{eff} \to n_0$ the scaled spin-orbit splitting and the physical value coincide leading to a good agreement of physical and scaled spectra in this energy range. Contrary to the physical spectrum, the scaled spectrum can be understood directly in terms of classical orbits, because the semiclassical density of states for

the scaled systems is given as a Fourier series with the semiclassical amplitudes $\mathcal{A}_{\mathrm{PO}}$ at positions $\tilde{S}_{\mathrm{PO}}$.

The scaled quantum spectrum shown in Fig. 1(a) is a sum of δ distributions, and thus the Fourier transform (FT) can easily be carried out analytically. The resulting Fourier spectrum is presented as black solid line in Fig. 1(b). It exhibits a large number of sharp peaks with increasing density as a function of $\tilde{S}$. The peaks should approach δ functions, i.e., become infinitely narrow for the Fourier transform of an infinitely long scaled quantum spectrum with $n_{\mathrm{eff}} \to \infty$. However, for finite length, resulting from the diagonalization of the truncated generalized eigenvalue problem [Eq. (7)], the peaks are broadened and side peaks may occur. To suppress these features we use a Gaussian window function as an envelope when performing the Fourier transform (Sec. III, Supplemental Material [17]).

For comparison, the semiclassical results are shown in Fig. 1(b) as colored peaks at the positions $\tilde{S}_{\mathrm{PO}}/2\pi$ of the periodic orbits. The peak heights mark the absolute values $|\mathcal{A}_{\mathrm{PO}}|$ of the semiclassical amplitudes. The peaks are labeled by the one to three winding numbers M_i of the corresponding periodic orbits moving on one- to three-dimensional tori. As can be seen in Fig. 1(b), the quantum mechanical and semiclassical exciton recurrence spectra agree very well. At low action ($\tilde{S}/2\pi \lesssim 5$) the peaks solely belong to one or multiple recurrences of the two shortest periodic exciton orbits, viz. the nearly circular orbits in the planes perpendicular to the [001] and [011] axes, moving on one-dimensional tori labeled by a single winding number $M_1 = 1, 2, 3, \ldots$. These orbits are shown in Fig. 2(a). At higher action ($\tilde{S}/2\pi \gtrsim 5$) the recurrence spectrum becomes more and more complicated due to the appearance of additional peaks belonging to exciton orbits on two-dimensional tori located in the planes perpendicular to the [001] and [011] axes (marked by two winding numbers $M_1 : M_2$) or fully three-dimensional orbits with winding numbers $M_1 : M_2 : M_3$. The 2D orbits with $M_1 : M_2 = 7 : 1$ in the symmetry planes of the crystal are shown in Fig. 2(b). Two fully 3D exciton orbits are illustrated in Figs. 2(c) and 2(d).

The structure of the classical exciton dynamics is illustrated in more detail in Fig. 3, where the classical action $\tilde{S}_{\mathrm{PO}}$ of the period orbits is shown as function of the ratio of the winding numbers M_1/M_2. For better visibility, the actions are normalized by the actions $\tilde{S}_{\perp[011]}$ of the corresponding orbits with the same winding numbers M_1 and M_2 in the plane perpendicular to the [011] axis. Therefore, by construction, the periodic orbits in the plane perpendicular to the [011] axis are located on the straight line at $\tilde{S}_{\mathrm{PO}}/\tilde{S}_{\perp[011]} = 1$. These orbits lie on a 2D torus in phase space. With increasing ratio M_1/M_2 they converge at $M_1/M_2 \approx 68.8$ to the nearly circular orbit in the symmetry plane perpendicular to [011]. This point in Fig. 3 thus represents a limiting 1D torus in phase space indicated by the green rhombus. In a similar way the periodic orbits perpendicular to the [001] axis, lying on a different 2D torus in phase space, are located on the upper line in Fig. 3 with the limiting nearly circular orbit on a 1D torus at $M_1/M_2 \approx 44.8$ shown as a blue rhombus. In between the orbits on the two limiting 2D tori the periodic orbits on the 3D tori are located. Subsets of these orbits with winding
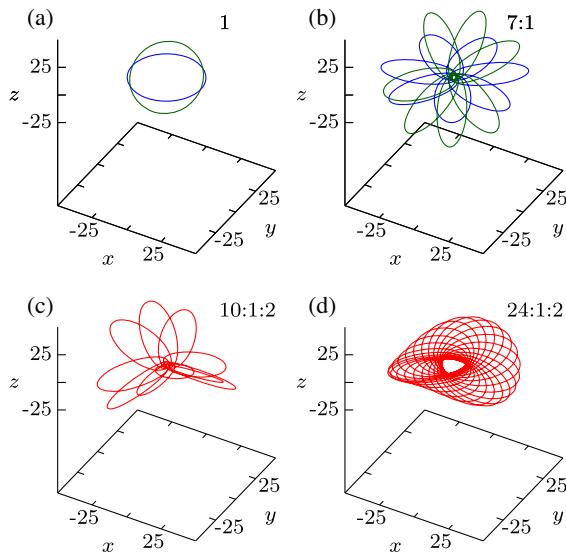
FIG. 2. (a) Nearly circular orbits with winding number $M_1 = 1$ and (b) planar orbits with winding numbers $M_1 : M_2 = 7 : 1$ in the two different symmetry planes of the crystal. (c), (d) Two examples of fully three-dimensional orbits with winding numbers $M_1 : M_2 : M_3$. The colors are the same as in Fig. 1.
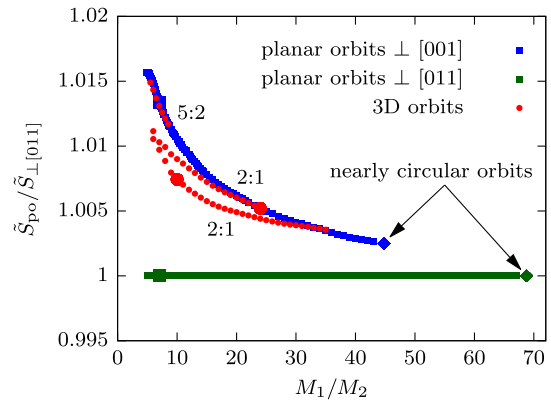
FIG. 3. Actions $\tilde{S}_{\mathrm{PO}}$ of periodic orbits as function of the ratio of winding numbers M_1/M_2. The actions are normalized by the actions $\tilde{S}_{\perp[011]}$ of the corresponding orbits with the same winding numbers M_1 and M_2 in the plane perpendicular to the [011] axis. The two-dimensional orbits approach the action of the nearly circular orbit (indicated by rhombi) of the corresponding plane with increasing M_1/M_2. Some three-dimensional orbits with marked ratio $M_3 : M_2$ are located in the area enclosed by orbits in the two different symmetry planes of the O_h group. The orbits shown in Fig. 2 are highlighted by larger symbols.

number $M_2 = 1$ or 2 and ratios $M_3 : M_2 = 2 : 1$ or $5 : 2$ are marked by red dots in Fig. 3. The three-dimensional orbits fill the area between the limiting 2D tori more densely when longer periodic orbits with more complicated ratios of the winding numbers are considered. As can be seen in Fig. 3, the classical action of periodic orbits with the same winding numbers M_1 and M_2 differ by less than 2%. This causes a clustering of several orbits in the recurrence spectra in Fig. 1(b). In these clusters the peaks at the highest action belong to the two-dimensional orbits in the (mostly) stable symmetry plane perpendicular to the [001] axis and its equivalents. Typically, these peaks exhibit the highest semiclassical amplitude within the cluster. At slightly lower action one finds unstable three-dimensional orbits, and the peak with lowest action of the cluster belongs to a two-dimensional orbit in the plane perpendicular to the [011] axis.

In summary, we have found signatures of exciton orbits in quantum mechanical recurrence spectra of cuprous oxide. We have revealed the classical phase space structure of yellow excitons in cuprous oxide and observed recurrence peaks in Fourier transform quantum spectra, which, by application of semiclassical theories can be directly related to two-dimensional periodic orbits in symmetry planes of the crystal or fully three-dimensional periodic orbits. The results have been obtained by using an adiabatic approach for the classical exciton dynamics and by application of a scaling technique to the quantum spectra. Considering these approximations and that the Bohr-Sommerfeld model already fails to predict the energy levels of the helium atom, it is remarkable that a classical picture is capable of describing the spectral features of excitons in Cu_2O. Here, we have focused on the dynamics of Rydberg excitons with principal quantum number $n = 5$ in the (nonscaled) Cu_2O crystal. The analysis will be extended to other dynamics regimes by varying n_0. It will also be interesting to investigate the classical and semiclassical dynamics of magnetoexcitons [33,34] in cuprous oxide. Furthermore, the classical model intrinsically exhibits a dipole moment which could provide a starting point to describe and better understand interactions between Rydberg excitons such as scattering processes between Rydberg excitons [35,36], the Rydberg blockade [37], and the possible existence of an exciton molecule [38] in analogy to Rydberg molecules [39,40].

---

*main@itp1.uni-stuttgart.de

[1] E. F. Gross, Optical spectrum of excitons in the crystal lattice, Nuovo Cimento (1955–1965) **3**, 672 (1956).

[2] J. M. Luttinger, Quantum theory of cyclotron resonance in semiconductors: General theory, Phys. Rev. **102**, 1030 (1956).

[3] T. Kazimierczuk, D. Fröhlich, S. Scheel, H. Stolz, and M. Bayer, Giant Rydberg excitons in the copper oxide Cu_2O, Nature (London) **514**, 343 (2014).

[4] F. Schöne, S.-O. Krüger, P. Grünwald, M. Aßmann, J. Heckötter, J. Thewes, H. Stolz, D. Fröhlich, M. Bayer, and S. Scheel, Coupled valence band dispersions and the quantum defect of excitons in Cu_2O, J. Phys. B **49**, 134003 (2016).

[5] F. Schöne, S.-O. Krüger, P. Grünwald, H. Stolz, S. Scheel, M. Aßmann, J. Heckötter, J. Thewes, D. Fröhlich, and M. Bayer, Deviations of the exciton level spectrum in Cu_2O from the hydrogen series, Phys. Rev. B **93**, 075203 (2016).

[6] J. Thewes, J. Heckötter, T. Kazimierczuk, M. Aßmann, D. Fröhlich, M. Bayer, M. A. Semina, and M. M. Glazov, Observation of High Angular Momentum Excitons in Cuprous Oxide, Phys. Rev. Lett. **115**, 027402 (2015).

[7] F. Schweiner, J. Main, M. Feldmaier, G. Wunner, and C. Uihlein, Impact of the valence band structure of Cu_2O on excitonic spectra, Phys. Rev. B **93**, 195203 (2016).

[8] F. Schweiner, J. Main, G. Wunner, and C. Uihlein, Even exciton series in Cu_2O, Phys. Rev. B **95**, 195201 (2017).

[9] M. V. Berry and M. Tabor, Closed orbits and the regular bound spectrum, Proc. R. Soc. A **349**, 101 (1976).

[10] M. C. Gutzwiller, *Chaos in Classical and Quantum Mechanics* (Springer, New York, 1990).

[11] F. Haake, S. Gnutzmann, and M. Kuś, *Quantum Signatures of Chaos, Fourth Edition*, Springer Series in Synergetics (Springer, Cham, 2018).

[12] H. Friedrich and H. Wintgen, The hydrogen atom in a uniform magnetic field—An example of chaos, Phys. Rep. **183**, 37 (1989).

[13] H. Hasegawa, M. Robnik, and G. Wunner, Classical and quantal chaos in the diamagnetic Kepler problem, Prog. Theor. Phys. Suppl. **98**, 198 (1989).

[14] J. Ertl, P. Rommel, M. Mom, J. Main, and M. Bayer, Classical and semiclassical description of Rydberg excitons in cuprous oxide, Phys. Rev. B **101**, 241201(R) (2020).

[15] S. Gekle, J. Main, T. Bartsch, and T. Uzer, Extracting Multidimensional Phase Space Topology from Periodic Orbits, Phys. Rev. Lett. **97**, 104101 (2006).

[16] S. Gekle, J. Main, T. Bartsch, and T. Uzer, Hydrogen atom in crossed electric and magnetic fields: Phase space topology and torus quantization via periodic orbits, Phys. Rev. A **75**, 023406 (2007).

[17] See Supplemental Material at http://link.aps.org/supplemental/10.1103/PhysRevLett.129.067401 for Sec. I, which provides details on semiclassical periodic orbit theory including semiclassical density of states, scaling techniques, and recurrence spectra, and includes the additional Refs. [18,19]; Sec. II, which provides details on the computation of classical dynamics and the application of semiclassical methods for excitons in cuprous oxide, and includes the additional Ref. [20]; and Sec. III, which provides details on the computation of the scaled quantum mechanical density of states and scaled recurrence spectra for excitons in cuprous oxide, and includes the additional Refs. [21–25].

[18] P. Cvitanović and B. Eckhardt, Periodic-Orbit Quantization of Chaotic Systems, Phys. Rev. Lett. **63**, 823 (1989).

[19] A. Holle, J. Main, G. Wiebusch, H. Rottke, and K. H. Welge, Quasi-Landau Spectrum of the Chaotic Diamagnetic Hydrogen Atom, Phys. Rev. Lett. **61**, 161 (1988).

[20] M. Schumacher, Semiclassical analysis and interpretation of quantum mechanically computed Cu_2O exciton spectra, Master's thesis, Universität Stuttgart, 2021.

[21] M. A. Caprio, P. Maris, and J. P. Vary, Coulomb-Sturmian basis for the nuclear many-body problem, Phys. Rev. C **86**, 034312 (2012).

[22] B. Klahn and W. A. Bingel, The convergence of the Rayleigh-Ritz method in quantum chemistry I., Theor. Chim. Acta **44**, 9 (1977).

[23] B. Klahn and W. A. Bingel, The convergence of the Rayleigh-Ritz method in quantum chemistry II., Theor. Chim. Acta **44**, 27 (1977).

[24] G. Koster, J. Dimmock, R. Wheeler, and H. Statz, *Properties of the Thirty-Two Point Groups*, Massachusetts Institute of Technology Press research monograph (M.I.T. Press, Cambridge, 1963).

[25] E. Anderson, Z. Bai, C. Bischof, S. Blackford, J. Demmel, J. Dongarra, J. D. Croz, A. Greenbaum, S. Hammarling, and A. McKenney, *LAPACK Users' Guide*, Third edition (Society for Industrial and Applied Mathematics, Philadelphia, 1999).

[26] J. Main, Use of harmonic inversion techniques in semiclassical quantization and analysis of quantum spectra, Phys. Rep. **316**, 233–338 (1999).

[27] N. O. Lipari and M. Altarelli, Theory of indirect excitons in semiconductors, Phys. Rev. B **15**, 4883 (1977).

[28] C. Uihlein, D. Fröhlich, and R. Kenklies, Investigation of exciton fine structure in Cu_2O, Phys. Rev. B **23**, 2731 (1981).

[29] P. Rommel, P. Zielinski, and J. Main, Green exciton series in cuprous oxide, Phys. Rev. B **101**, 075208 (2020).

[30] A. Farenbruch, D. Fröhlich, D. R. Yakovlev, and M. Bayer, Rydberg Series of Dark Excitons in Cu_2O, Phys. Rev. Lett. **125**, 207402 (2020).

[31] P. Rommel, J. Main, A. Farenbruch, D. R. Yakovlev, and M. Bayer, Exchange interaction in the yellow exciton series of cuprous oxide, Phys. Rev. B **103**, 075202 (2021).

[32] S. Tomsovic, M. Grinberg, and D. Ullmo, Semiclassical Trace Formulas of Near-Integrable Systems: Resonances, Phys. Rev. Lett. **75**, 4346 (1995).

[33] F. Schweiner, J. Main, G. Wunner, M. Freitag, J. Heckötter, C. Uihlein, M. Aßmann, D. Fröhlich, and M. Bayer, Magnetoexcitons in cuprous oxide, Phys. Rev. B **95**, 035202 (2017).

[34] F. Schweiner, J. Main, and G. Wunner, Magnetoexcitons Break Antiunitary Symmetries, Phys. Rev. Lett. **118**, 046401 (2017).

[35] Y. Hefetz, X.-C. Zhang, and A. V. Nurmikko, Observation of exciton-exciton scattering in Cu_2O by time-resolved photomodulation spectroscopy, Phys. Rev. B **31**, 5371 (1985).

[36] J. Shumway and D. M. Ceperley, Quantum Monte Carlo treatment of elastic exciton-exciton scattering, Phys. Rev. B **63**, 165209 (2001).

[37] J. Heckötter, V. Walther, S. Scheel, M. Bayer, T. Pohl, and M. Aßmann, Asymmetric Rydberg blockade of giant excitons in cuprous oxide, Nat. Commun. **12**, 3556 (2021).

[38] F. Bassani and M. Rovere, Biexciton binding energy in Cu_2O, Solid State Commun. **19**, 887 (1976).

[39] V. Bendkowsky, B. Butscher, J. Nipper, J. P. Shaffer, R. Löw, and T. Pfau, Observation of ultralong-range Rydberg molecules, Nature (London) **458**, 1005 (2009).

[40] A. Junginger, J. Main, and G. Wunner, Quantum-classical model for the formation of Rydberg molecules, Phys. Rev. A **86**, 012713 (2012).